Materials Science Forum
ISSN: 1662-9752, Vol. 1190, pp 27-35
doi:10.4028/p-5mleKn

Submitted: 2025-09-12
Revised: 2026-01-18
Accepted: 2026-03-21
Online: 2026-05-18

Trial Implementation of Operando PL Spectrum Mapping Using a Mini-Spectrometer in EVC Screening of 4H-SiC Wafers

Kazumi Takano[1,a*], Yasuyuki Igarashi[1,b], Yohsuke Matsushita[1,c] and Takuya Morita[1,d]

[1]ITES, 1-60 Kuribayashi, Otsu, Shiga 520-2151, Japan

[a*]kazumi_takano@ites.co.jp, [b]yiga@ites.co.jp, [c]yohsuke_matsushita@ites.co.jp, [d]takuya_morita@ites.co.jp

Keywords: PL mapping, proton implantation, Shockley-type stacking fault (SSF), photoluminescence (PL), UV irradiation, basal plane dislocation (BPD).

Abstract. We have been developing the expansion–visualization–contraction (EVC) method as an inspection technique for 4H-SiC wafers, in which Shockley-type stacking faults (SSFs) are intentionally expanded by UV irradiation and subsequently visualized to identify converted dislocations that are not directly detectable by conventional PL inspection. In this study, we demonstrate a low-cost "operando" PL spectrum mapping approach for the EVC tool by using the 355-nm expansion laser as the PL excitation source and adding only a miniature spectrometer via an optical fiber, avoiding the need for an expensive hyperspectral camera. Two experiments were performed. In Experiment 1, proton-implanted and non-implanted regions on n-type 4H-SiC epilayers were compared using EVC screening and PL imaging. The proton-implanted regions exhibited narrower SSF widths, and a two-sample t-test yielded extremely small p-values, indicating a statistically significant suppression effect that remained after activation annealing. In Experiment 2, a thick epilayer wafer containing polytype inclusions was screened. PL spectrum mapping identified not only 1SSF-related emission (~420 nm) but also Frank-type components (~488 nm) and polytype-inclusion-related emission (~540 nm), revealing composite stacking faults expanded from inclusions. The results suggest that operando PL spectrum mapping can help distinguish stacking-fault types during EVC screening and potentially prevent unnecessary expansion of thermally uncontractable faults, thereby reducing yield loss.

Introduction

We have been developing the EVC (Expansion–Visualization–Contraction) method as an inspection technique for 4H-SiC wafers [1]. In industry, photoluminescence (PL) inspection is widely used as one of the standard methods for evaluating 4H-SiC wafers and epitaxial layers [2]. PL inspection is effective for detecting basal plane dislocations (BPDs) in epitaxial layers; however, it cannot directly detect BPDs that convert into threading edge dislocations (TEDs) at the substrate/epilayer interface (i.e., BPD-origin TEDs). Both through-going BPDs and converted BPD-origin TEDs can trigger the expansion of stacking faults during current-induced degradation [3], and therefore both types of defects can critically affect the reliability and yield of final products.

To address this limitation, we propose to inspect BPD-origin TEDs—undetectable by conventional PL inspection—using the EVC screening method. The EVC screening method consists of three steps: (i) an Expansion step, in which SSFs are intentionally expanded in the epilayer by ultraviolet (UV) irradiation; (ii) a Visualization step, in which the converted dislocation is not directly observed but is instead identified as the source of Shockley stacking faults (SSFs); and (iii) a Contraction step, in which the expanded SSFs are contracted to recover wafer quality [1].

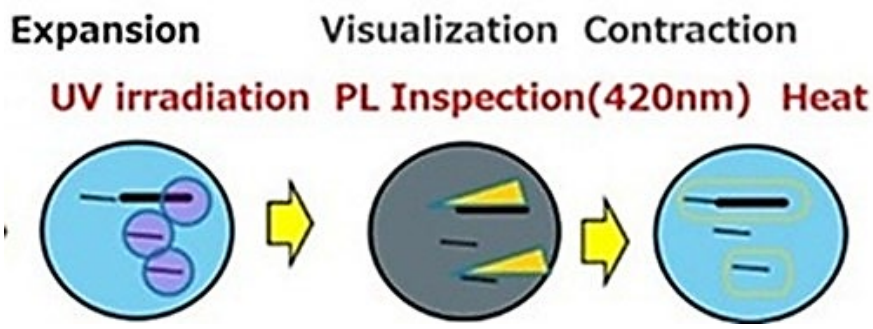

Fig. 1. EVC Screening method.

Operando approaches have been reported for studying current-induced degradation in SiC devices. Because a biased device generally emits electroluminescence (EL), in-situ EL observation is possible in principle; however, observation is often hindered by metal electrodes. To overcome this, a method using comb-shaped electrodes has been proposed so that EL can be observed through open windows [4]. In addition, combined schemes have been reported in which the current stress is temporarily stopped and PL imaging is performed in between stress intervals [5]. Current-stress-based SSF expansion has the advantage of applying stress in a structure close to the final product. Nevertheless, it requires electrode fabrication and other processing steps starting from a bare wafer, which increases both time and cost. Moreover, when the SSF expansion is driven by wafer-origin BPDs, performing operando characterization directly at the wafer stage may reduce disturbances introduced by electrodes and electrical circuitry. For example, series resistance in electrodes can reduce the injected current, decrease the EL intensity, and potentially lead to misclassification. In-situ PL observation, on the other hand, typically requires a dedicated excitation source, microscope optics, and a 2D camera, resulting in a more complex and costly instrumentation.

In the EVC tool, operando PL observation is, in principle, achievable by alternating the Expansion and Visualization steps. However, implementing a mechanical system that repeatedly moves the wafer while maintaining high positional accuracy significantly increases cost. In this study, we exploit the fact that the third harmonic of a YAG laser (e.g., 355 nm) used in the Expansion step can also serve as a PL excitation source. We investigate the feasibility of low-cost operando PL spectrum mapping [6] by adding only a miniature spectrometer, without employing an expensive hyperspectral camera. The ability to acquire PL spectrum mapping data at low cost is particularly attractive under limited development budgets.

Furthermore, if SF types can be identified from PL spectra, unnecessary expansion of SFs that are difficult to contract thermally (e.g., Frank-type faults) could be avoided, thereby preventing reduction of usable wafer area.

This paper reports a trial implementation of operando PL spectrum mapping as a pathway to enhance the functionality of the EVC tool. Specifically, we demonstrate the influence of activation annealing on proton-implanted wafers prior to electrode formation, and present an example of detecting Frank-type SSFs that are difficult to contract.

Experimental Preparation: Installation of a Mini-Spectrometer

A quartz optical fiber for collecting PL emission was mounted near the UV-laser irradiation spot used for SSF expansion. The fiber was connected to a compact multichannel Si-CCD spectrometer (FLAME-S, Ocean Optics; wavelength range: 220–850 nm) for PL spectral measurements (Fig. 2).

Experiment 1: EVC Screening and PL Spectroscopy

Samples and proton implantation

Three commercial n-type 4H-SiC epitaxial wafers with a 4° off-cut were used in this study. The epitaxial structures are summarized in Table 1. Proton implantation was carried out from the epilayer surface under the conditions listed in Table 1. The projected implantation depths for wafers A and B

were calculated using SRIM2013 [7], and the results are shown in Fig. 4. For wafer C, protons were accelerated to 2 MeV and then decelerated by passing through an aluminum foil, adjusting the effective energies to the equivalent of 1.25 MeV and 600 keV. Fig. 3 shows the damage events calculated using SRIM2013.

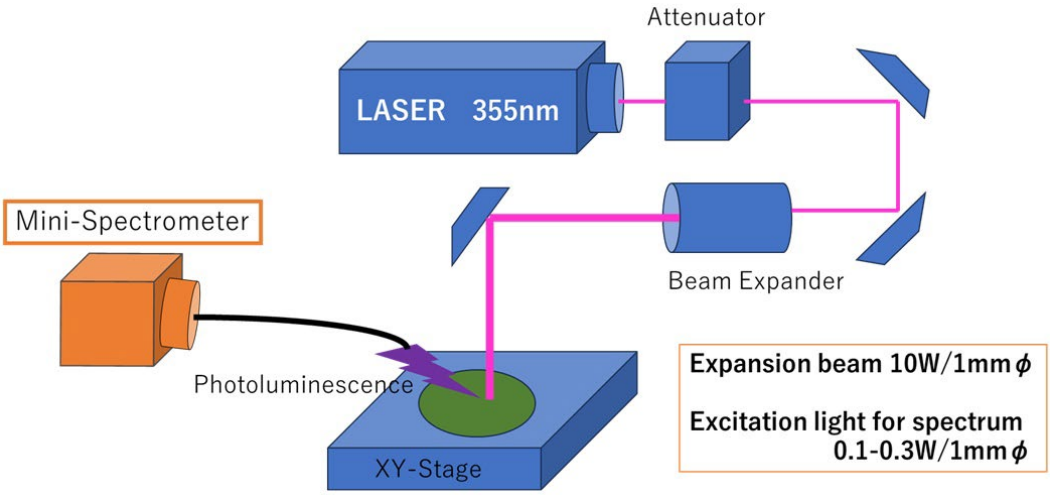

Fig. 2. Expansion process.

Table 1. Wafers.

	Active	Buffer layer		Drift Layer		Proton Implantation	
	Annealing	Thickness (um)	ND (cm^{-3})	Thickness (um)	ND (cm^{-3})	(keV)	ND (cm^{-2})
Wafer A	YES	1	1.00E+18	10	8.00E+15	350	1.00E+13
Wafer B	NO	0.5	1.00E+18	8	1.00E+16	600	1.40E+14
Wafer C	YES	3	1.00E+18	19	4.00E+15	600, 1250	1.00E+12

Expansion step (UV-irradiation)

As an expansion step, wafers A and B were irradiated by a scanned UV laser over a 10×10 mm^2 area spanning both the proton-implanted and non-implanted regions in order to induce and expand Shockley-type stacking faults (SSFs) (Fig. 3).

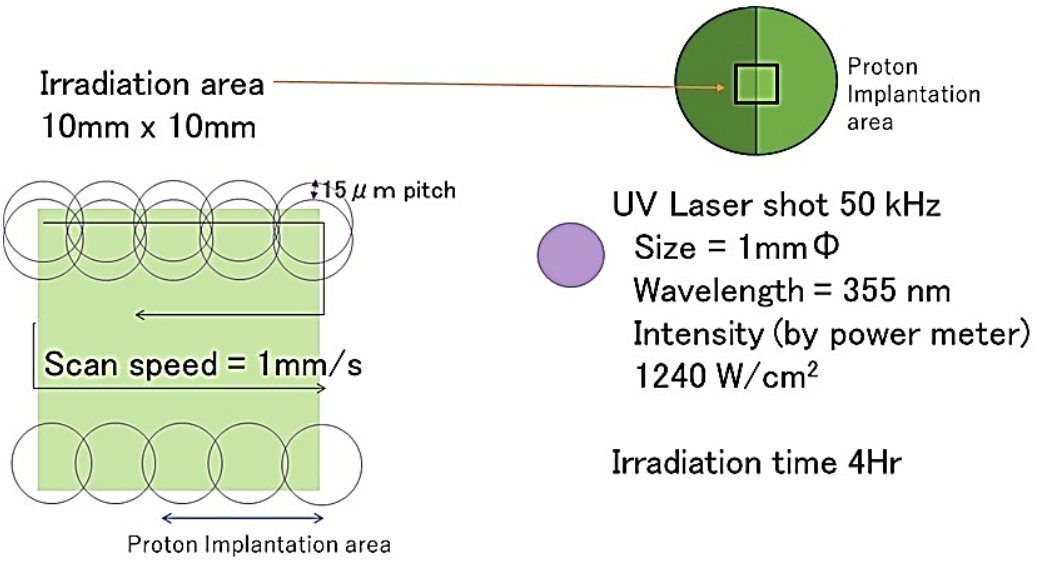

Fig. 3. UV irradiation.

Visualization step (PL imaging and SSF-width analysis)

As a visualization step, the expanded SSFs were evaluated by PL imaging. The SSF widths in the proton-implanted and non-implanted regions were measured, and a two-sample t-test was performed to assess the difference in mean SSF width between the two regions. By comparing wafers A and B, we examined whether the SSF-expansion suppression effect of proton implantation is maintained after activation annealing (i.e., not deactivated by the annealing process).

Contraction step and reproducibility check

As a contraction step, wafer B was annealed at 800 °C for 3 h to contract the expanded SSFs. The expansion and visualization steps were then repeated to evaluate the reproducibility of SSF initiation locations. This procedure was conducted to confirm that the EVC screening method does not adversely affect wafer quality.

PL spectroscopy for wafer-quality evaluation

Using wafer C, PL spectra were measured before proton implantation, after proton implantation, and after activation annealing in order to evaluate changes in wafer quality associated with each processing step.

Result 1: EVC Screening and PL Spectroscopy

Simulations by SRIM2013 [7]

SRIM2013 simulations suggested that implanted protons accumulate at a depth of approximately 2.4 μm in wafer A and approximately 5 μm in wafer B (Fig. 4). Fig. 5 shows the vacancy concentration estimated from SRIM2013 calculations for proton implantation.

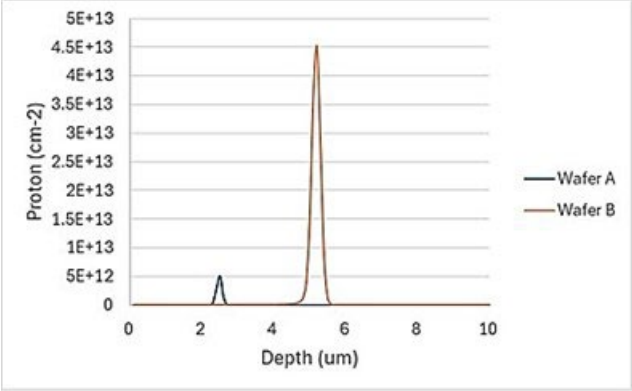

Fig. 4. Proton Distribution.

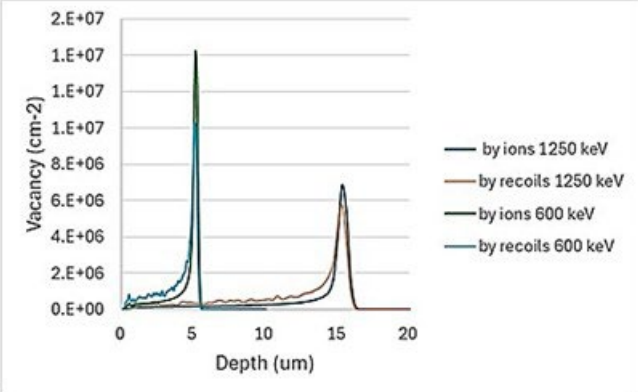

Fig. 5. Vacancy Distribution.

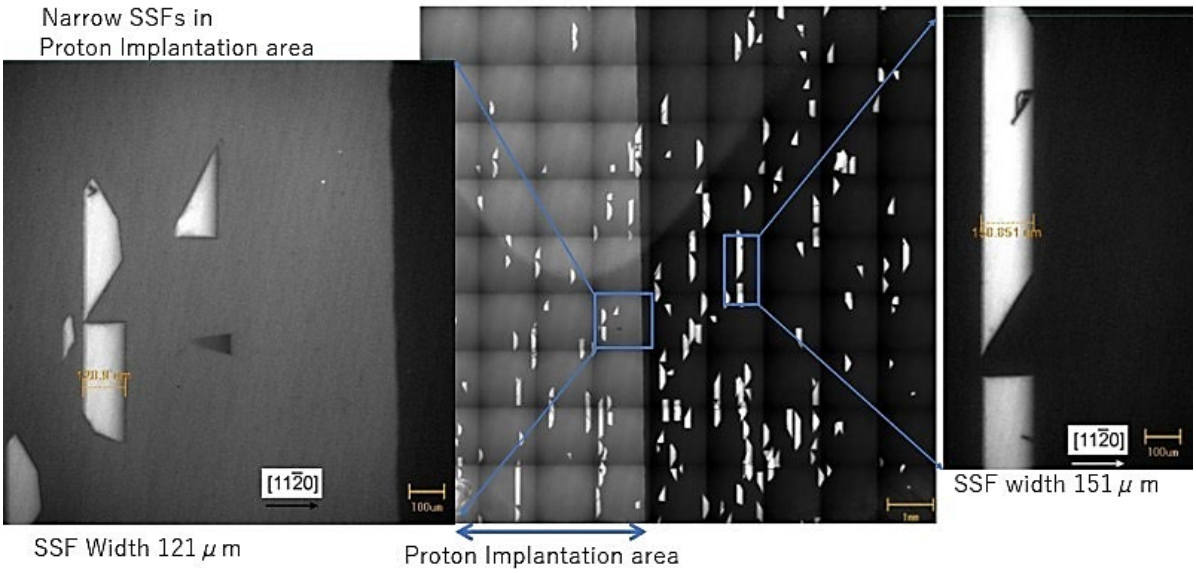

Fig. 6. PL Images of Wafer A.

UV-PL imaging of expanded SSFs

Fig. 6 shows UV-PL images of SSFs expanded by the EVC procedure for wafer A. The SSFs in the proton-implanted region exhibited a narrower band width than those in the non-implanted region, indicating that proton implantation suppresses SSF expansion.

Repeatability of SSF expansion after contraction

Fig. 7 shows UV-PL images acquired using a 420-nm band-pass filter (BPF420). The white regions correspond to SSFs. The lower half of the image is the proton-implanted area, where SSFs were observed as gray features against a darker background. Panel (a) corresponds to the first expansion step. After the contraction step, the white SSF contrast disappeared (b). Panel (c) shows the second expansion step, in which SSFs expanded again at the same locations. The white square feature in the lower right region was not an SSF and was attributed to contamination.

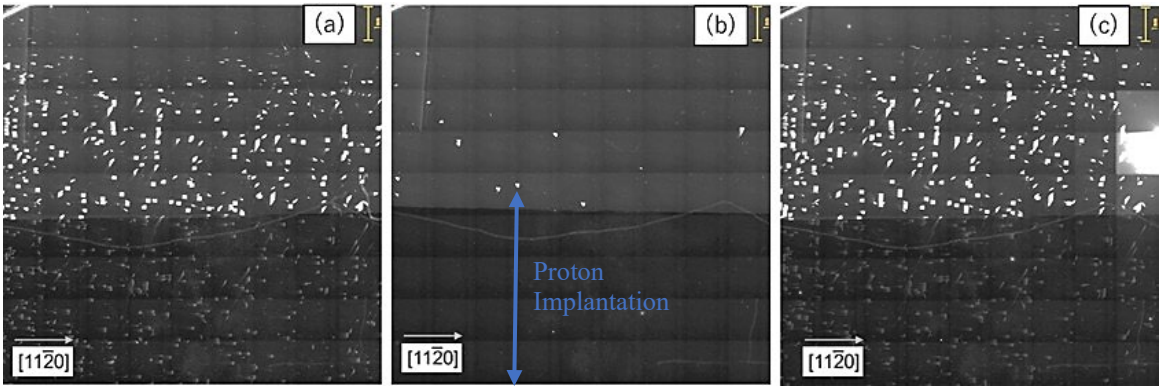

1st UV Irradiation Contraction 2nd UV Irradiation

Fig. 7. PL Images of Wafer B.

Statistical comparison of SSF widths

Ten stripe-like SSFs were selected from each area, and their widths were measured. For both proton-implanted wafer A and wafer B, the SSF widths in the epilayer differed between the proton-implanted and non-implanted regions. A two-sample t-test yielded extremely small p-values (Table 2), indicating a statistically significant difference. These results suggest that the SSF-expansion suppression effect appears immediately after proton implantation and remains effective even after activation annealing.

Table 2. T-TEST.

Wafer	Proton	Average of SSF wideth (μm)	Standard deviation	Difference in means	P value	95% CI diff (equal var)
A	NO	150.3	1.52	28.2	1.03E-17	26.4, 30.0
	YES	122.1	2.17			
B	NO	120.6	2.58	72.8	2.07E-24	70.9, 74.7
	YES	47.8	1.29			

Reproducibility of SSF initiation locations

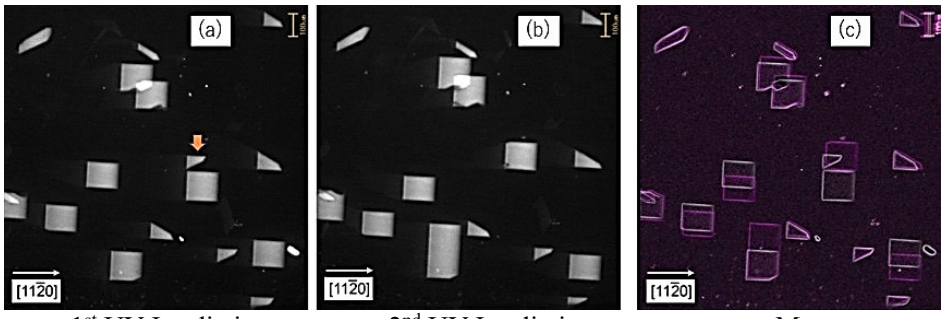

1st UV Irradiation 2nd UV Irradiation Montage

Fig. 8. PL Images of Wafer B.

Fig. 8(a) shows the UV-PL image obtained after the first expansion step, while Fig. 8(b) shows the UV-PL image obtained after the second expansion step following a contraction process. For comparison, the extracted contours from (b) were colored in purple and overlaid onto (a), as shown in Fig. 8(c). Sixteen SSFs were observed after the first expansion, and fifteen SSFs were observed after the second expansion at nearly the same locations. This reproducibility suggests that the EVC procedure does not measurably degrade wafer quality under the present conditions.

PL spectra

The PL spectra in Fig. 9 are consistent with the above EVC-based evaluation of proton implantation. The emergence of the SSF-expansion suppression effect after proton implantation agrees with the reduced intensity of the band-to-band emission peak at 390 nm following implantation. In addition, the persistence of the suppression effect after activation annealing is consistent with the observation that the 390-nm peak intensity decreased slightly after annealing but remained largely stable overall.

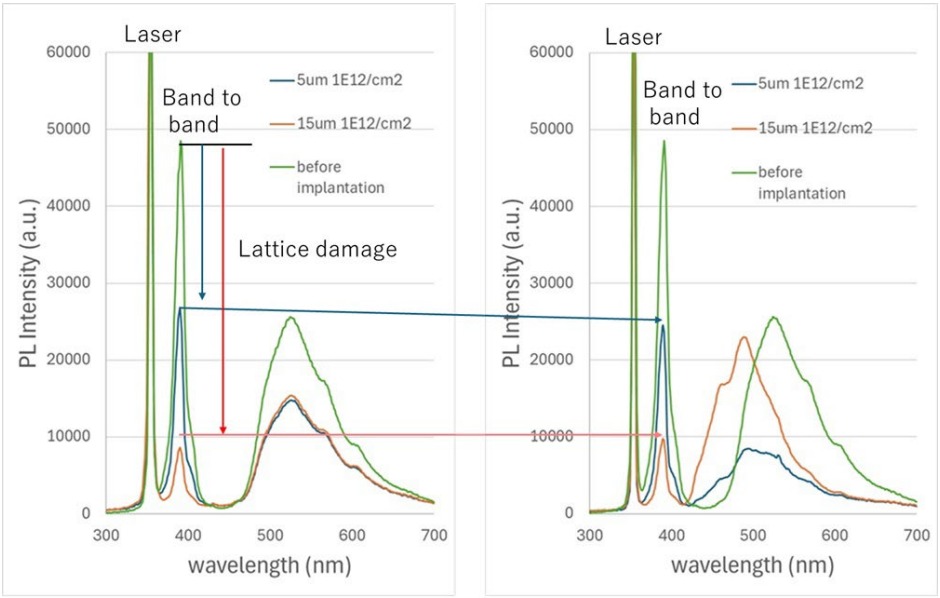

a) After proton Implantation b) After active anneal

Fig. 9. PL spectrum of Wafer C.

Experiment and Result 2: EVC Screening of Polytype-Inclusion-Related Stacking Faults and in situ PL Spectral Mapping

An epitaxial wafer containing multiple polytype inclusions was purchased (Fig. 10). The wafer was an n-type 150-mm-diameter 4H-SiC epitaxial wafer with a 4° off-cut, consisting of a heavily nitrogen-doped buffer layer (2 μm, 1×10^{18} cm^{-3}) and a lightly doped drift layer (60 μm, 9×10^{14} cm^{-3}).

Focusing on regions containing triangular stacking faults (SFs), we evaluated the wafer using the EVC screening. After 355-nm laser irradiation as the expansion step, UV-PL imaging with a 420-nm band-pass filter (BPF420) was performed as the visualization step, and numerous bar-shaped SFs were observed. At this stage, as a simulated operando observation, PL spectral mapping was carried out within the yellow dashed region in Fig. 12 The measurement was performed with a 0.25-mm step while the laser irradiance was attenuated to approximately 1/100. Subsequently, a contraction step was conducted by annealing at 800 °C for 3 h.

Fig. 11(a) shows a bar-shaped 1SSF originating from a basal plane dislocation (BPD), whereas Fig. 11(b) shows a bar-shaped SF expanded from an inclusion containing SFs; its morphology was slightly different from that of the 1SSF in Fig. 11(a). After the contraction process, the 1SSF in Fig. 11(a) disappeared completely, whereas part of the SF in Fig. 11(b) remained uncontracted. No further change was observed even after an additional 6 h of annealing. The remaining SF is therefore considered to be different from a BPD-originated 1SSF.

Fig. 12(a) shows a PL image obtained with BPF420, and Fig. 12(b) shows the corresponding spectral mapping at 420 nm. Both images capture approximately two sets of bar-shaped stacking faults. Fig. 12(c) shows representative spectra; because both SSFs exhibit a peak at 420 nm, their dominant component was attributed to 1SSF.

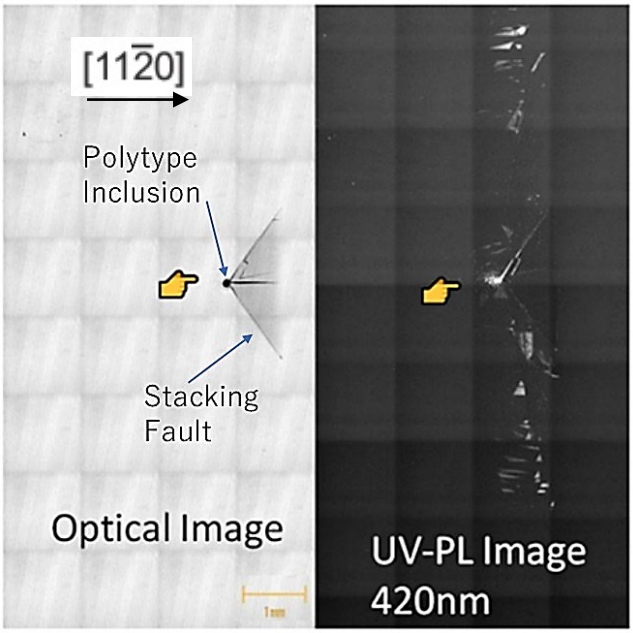

Fig. 10. Polytype inclusion with triangle SF.

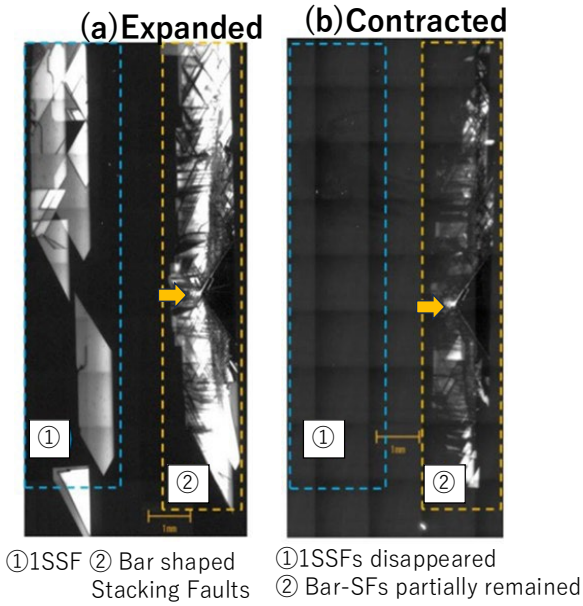

Fig. 11. PL image using BPF 420nm.

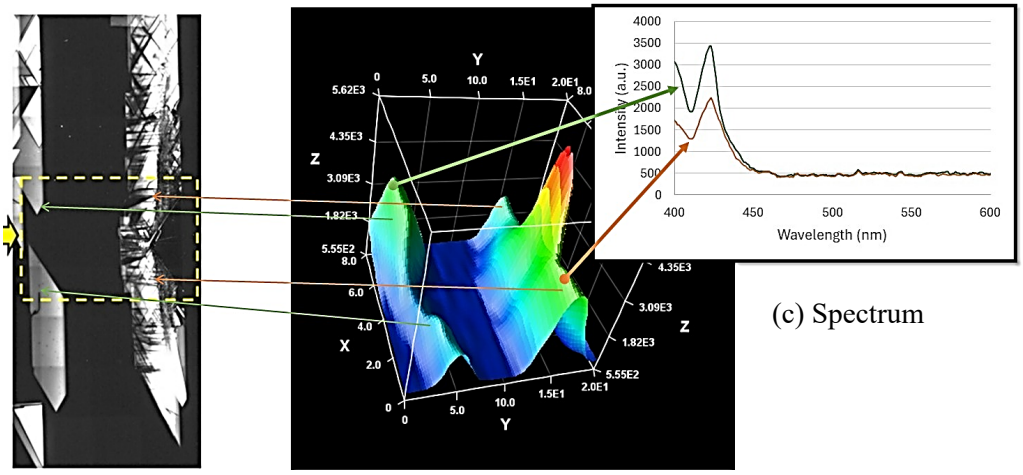

Fig. 12. (a) PL-imaging (b) PL-Spectrum (420 nm) mapping.

Fig. 13(a) shows a PL image obtained with BPF420, and Fig. 13(b) shows spectral mapping at 488 nm. The 488-nm mapping revealed enhanced intensity at SF positions connected to polytype inclusions. The spectra in Fig. 13(c) exhibit a 420-nm peak attributed to 1SSF, a 488-nm peak attributed to Frank-type stacking faults [8], and a 540-nm peak attributed to polytype inclusions. These results indicate that stacking faults expanding from polytype inclusions are of a composite type, including not only 1SSF but also Frank-type stacking faults. If the uncontracted SFs are Frank-type faults with high thermal stability, their persistence after 800 °C annealing can be reasonably explained. These findings suggest that PL spectral mapping performed as an operando observation during EVC screening could enable early identification of SFs that do not contract (e.g., Frank-type components) and may allow their expansion to be halted at an early stage.

Because uncontractable SFs can render the affected wafer area unusable, minimizing their lateral extent is desirable from a cost perspective, and operando PL spectral mapping is therefore beneficial.

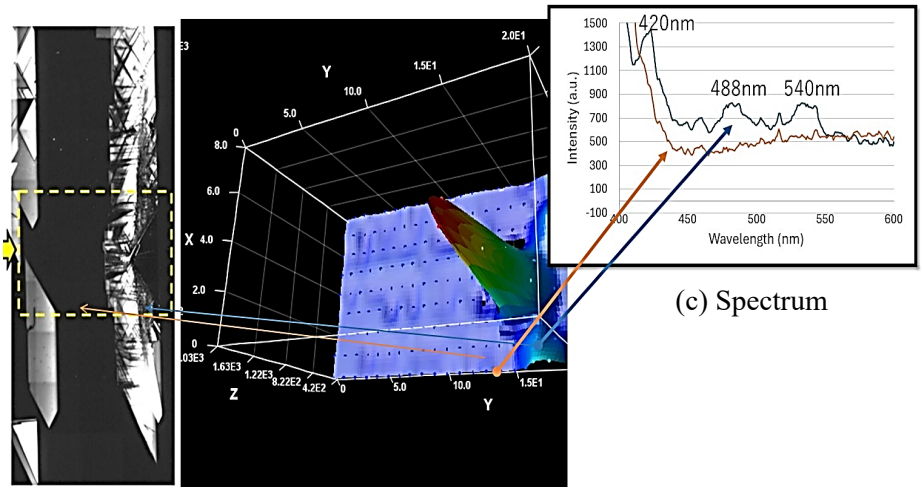

Fig. 13. (a) PL-imaging (b) PL-Spectrum (488 nm) mapping.

Conclusion

A miniature-spectrometer-based operando PL spectrum mapping scheme was implemented for the EVC inspection method by reusing the 355-nm expansion laser as the PL excitation source and collecting emission through an optical fiber. In proton-implanted epilayers, EVC/PL imaging showed a statistically significant reduction in SSF width, and the suppression effect persisted after activation annealing.

For a thick epilayer wafer containing polytype inclusions, PL spectrum mapping distinguished composite stacking faults expanded from inclusions, comprising 1SSF-related emission (~420 nm) together with Frank-type (~488 nm) and inclusion-related (~540 nm) components. These findings

indicate that low-cost operando PL spectrum mapping can enhance EVC screening by enabling early fault-type identification and by supporting strategies to avoid unnecessary growth of thermally persistent faults that can reduce usable wafer area.

Acknowledgment

METI R&D Support Program for Growth-oriented Technology SMEs Grant Number JPJ005698

References

[1] Y. Igarashi, K. Takano, Y. Matsushita, C. Shibata, Defect and Diffusion Forum Vol. 425, pp. 75-82 (2023).

[2] International Electrotechnical Commission Standard 63068-3 (2020).

[3] A. Tanaka, H. Matsuhata, N. Kawabata, D. Mori, K. Inoue, M. Ryo, T.Fujimoto, T. Tawara, M. Miyazato, M. Miyajima, K. Fukuda, A. Ohtsuki, T. Kato, H. Tsuchida, Y. Yonezawa, T. Kimoto, J. Appl. Phys. Vol. 99, 011101 (2006).

[4] C. Ota, J. Nishio, A. Okada, R. Iijima, 19th Conference on Defects, Vol.52, pp. 5109–5120 (2023).

[5] K. Konishi, R. Fujita, A. Shima, J. Electron. Mater. Vol. 48, pp. 1704–1713 (2019).

[6] G. Feng, J. Suda, T. Kimoto, Appl. Phys. Lett. Vol. 92, 221906 (2008).

[7] Information on http://www.srim.org/.

[8] S. Hageali, H. Guthrey, S. Johnston, A.Norman, J. Soto, B. Odekirk, R. Stahlbush, N. Mahadik, B. Gorman, M. Al-Jassim, J. Appl. Phys. Vol. 134, 075704 (2023).